ISSN 1674-1056
http://cpb.iphy.ac.cn
http://iopscience.iop.org/cpb
中国物理 B
Chinese Physics
中国物理
Chinese Physics B

Structural, Mössbauer spectroscopy, magnetic properties, and thermal measurements of $Y_{3-x}Dy_xFe_5O_{12}$

Mahdi Lataifeh, Qassem I Mohaidat, Sami H Mahmood, Ibrahim Bsoul, Mufeed Awawdeh, Ibrahim Abu-Aljarayesh, Mu'ath Altheeba

Citation: Chin. Phys. B . 2018, 27(10): 107501. **doi:** 10.1088/1674-1056/27/10/107501

Journal homepage: http://cpb.iphy.ac.cn; http://iopscience.iop.org/cpb

What follows is a list of articles you may be interested in

Effects of dipolar interactions on magnetic properties of Co nanowire arrays

Hong-Jian Li(李洪健), MingYue(岳明), Qiong Wu(吴琼), Yi Peng(彭懿), Yu-Qing Li(李玉卿), Wei-Qiang Liu(刘卫强), Dong-Tao Zhang(张东涛), Jiu-Xing Zhang(张久兴)
Chin. Phys. B . 2017, 26(11): 117503. **doi:** 10.1088/1674-1056/26/11/117503

Magnetic properties of Sn-substituted Ni–Zn ferrites synthesized from nano-sized powders of NiO, ZnO, Fe_2O_3, and SnO_2

M A Ali, M M Uddin, M N I Khan, F U Z Chowdhury, S M Hoque, S I Liba
Chin. Phys. B . 2017, 26(7): 077501. **doi:** 10.1088/1674-1056/26/7/077501

Low temperature ferromagnetic properties of CdS and CdTe thin films

Hafiz Tariq Masood, Zahir Muhammad, Muhammad Habib, Dong-Ming Wang(王东明), De-Liang Wang(王德亮)
Chin. Phys. B . 2017, 26(6): 067503. **doi:** 10.1088/1674-1056/26/6/067503

Structural and magnetic properties of turmeric functionalized $CoFe_2O_4$ nanocomposite powder

E Mehran, S Farjami Shayesteh, M Sheykhan
Chin. Phys. B . 2016, 25(10): 107504. **doi:** 10.1088/1674-1056/25/10/107504

Magnetocaloric and magnetic properties of La_2NiMnO_6 double perovskite

Masrour R, Jabar A
Chin. Phys. B . 2016, 25(8): 087502. **doi:** 10.1088/1674-1056/25/8/087502

Structural, Mössbauer spectroscopy, magnetic properties, and thermal measurements of $Y_{3-x}Dy_xFe_5O_{12}$*

Mahdi Lataifeh[1], Qassem I Mohaidat[1,†], Sami H Mahmood[2], Ibrahim Bsoul[3], Mufeed Awawdeh[1], Ibrahim Abu-Aljarayesh[1], and Mu'ath Altheeba[1]

[1] *Physics Department, Yarmouk University, Irbid* 21163, *Jordan*
[2] *Physics Department, The University of Jordan, Amman* 11942, *Jordan*
[3] *Physics Department, Al al-Bayt University, Mafraq* 13040, *Jordan*

(Received 6 January 2018; revised manuscript received 1 July 2018; published online 10 September 2018)

Yttrium iron garnet powder samples ($Y_{3-x}Dy_xFe_5O_{12}$), where part of yttrium ions are substituted by dysprosium ions with different concentrations are prepared by the solid state reaction method. The properties of the prepared samples are examined by different methods such as x-ray diffraction (XRD), Mössbauer spectroscopy, macroscopic magnetization measurements, and thermal measurements. The XRD measurements show that all the samples reveal the presence of a single garnet phase with a BCC structure. Room temperature Mössbauer spectra indicate that iron ions occupy three magnetic sites, i.e., two octahedral sites and one tetrahedral site. The saturation magnetization and the initial magnetic susceptibility decrease with the increase of Dy^{3+} substitution. The Curie temperature obtained from the thermal measurements seems to be independent of Dy^{3+} substitution.

Keywords: Mössbauer spectroscopy, magnetic properties, x-ray diffraction, differential scanning calorimetry

PACS: 75.60.Ej, 81.70.Pg, 82.80.Ej **DOI:** 10.1088/1674-1056/27/10/107501

1. Introduction

Ferrimagnetic garnets are isomorphic with the naturally occurring garnet $Ca_3Fe_2(SiO_4)_3$. Specifically, Yttrium iron garnet ($Y_3Fe_5O_{12}$, YIG) was discovered in 1956, and demonstrated suitability for high frequency microwave applications.[1–3] The discovery of YIG led to a revolution in the technological advancement of passive microwave devices including tunable filters, circulators, and gyrators, as well as magnetic-bubble-domain-type digital memory devices and other applications.[4–6]

The unit cell which has a cubic symmetry contains eight formula units of garnet, where the metal ions occupy three different interstitial sites. The Fe^{3+} ions occupy the 24*d* tetrahedrally coordinated sites and the 16*a* octahedrally coordinated sites, whereas the RE ions occupy the 24*c* dodecahedral sites. These latter sites are not all crystallographically equivalent, where six different *c* sites were reported.[7]

Since Y^{3+} is a nonmagnetic ion, the magnetization of YIG arises from the superexchange interaction between the moments of Fe^{3+} ions at *a* and *d* sublattices, resulting in a net magnetization of 5 μ_B per molecule at 0 K. When nonmagnetic Y^{3+} ions are substituted by heavy rare-earth (RE) ions from the series Gd^{3+} through Yb^{3+}, however, the magnetization as a function of temperature exhibits a compensation temperature (T_{comp}) at which the magnetization vanishes.[1,6] This is because these heavy RE elements are magnetic due to their unfilled 4*f* orbitals, introducing a third magnetic sublattice (*c*) which couples antiferromagnetically with the net magnetization of the Fe^{3+} sublattices due to the fact that the *a*–*d* superexchange interaction of Fe^{3+} ions is much stronger than the *a*–*c* or *d*–*c* interactions between Fe^{3+} and RE ions. Accordingly, such a substitution would facilitate the modifications of the magnetic properties of the garnet compounds, which renders these compounds attractive from the scientific and technological point of view. Further, the strong Fe–Fe interaction is responsible for the magnetic ordering of rare earth iron garnets (RIG), and the weak RE–Fe interactions make the Curie temperature of all rare-earth iron garnets nearly the same ($\sim$ 550 K).[8–10]

The effects of RE substitution for Y on the magnetic properties and hyperfine interactions in YIG garnets were investigated by several researchers. The saturation magnetization of $Y_{3-x}Dy_xFe_5O_{12}$ nanoparticles prepared by the sol-gel method was found to decrease linearly with increasing Dy^{3+} concentration (x) in a range between $0.0 \leq x \leq 1.0$, and increase with the increase of particle size.[11,12] Also, room temperature ^{57}Fe Mössbauer spectroscopy study of rare earth iron garnets $(R_xY_{1-x})_3Fe_5O_{12}$, where *R* is either Ho^{3+} or Gd^{3+}, has shown that the hyperfine field at the iron nucleus in the octahedral and tetrahedral sites increase with rare earth substitution.[13] On the other hand, room temperature Mössbauer spectroscopy indicated that Ho substitution for Y in YIG did not induce no-

*Project supported by the Deanship of Research and Graduate Studies of Yarmouk University (Garnet No. 33 /2015).
†Corresponding author. E-mail: q.muhaidat@yu.edu.jo
© 2018 Chinese Physical Society and IOP Publishing Ltd

ticeable changes in the hyperfine fields of the octahedral site nor tetrahedral sites.[14]

In this study, $Y_{3-x}Dy_xFe_5O_{12}$ powders are prepared by the solid state reaction method with part of Y ions being substituted by Dy ions in the full range between 0.0 and 3.0 ($x = 0.0, 0.5, 1.0, 1.5, 2.0, 2.5$, and 3.0). The structural and magnetic properties of the prepared compounds are investigated by x-ray diffraction (XRD), Mössbauer spectroscopy, and vibrating sample magnetometry (VSM). Also, differential scanning calorimetry is employed to investigate the Curie temperature of the compound. The interpretation of the magnetic results is based on the structural data and on the thermal measurements. This work is a continuation of our project involving the investigation of rare-earth iron garnets by several techniques such as nuclear magnetic resonance (NMR) of holmium in different RIG hosts,[10] Mössbauer spectroscopy,[13,14] and magnetization measurements.[8,9]

2. Experimental procedures

$Y_{3-x}Dy_xFe_5O_{12}$ powders with $x = 0.0$, 0.5, 1.0, 1.5, 2.0, 2.5, and 3.0 were prepared by the solid state reaction method. Metallic oxides Y_2O_3, Dy_2O_3, and Fe_2O_3 were used to fabricate $Y_{3-x}Dy_xFe_5O_{12}$ powder samples. Stoichiometric ratios of the metallic oxides were loaded into a hardened stainless steel cup with a ball-to-powder ratio of 8:1. The milling process was carried out at 250 rpm for 16 h. The resulting precursor was annealed at 1300 °C for 2 h. The XRD patterns were collected using a Philips X'pert PRO X-ray diffractometer (PW3040/60) operating at (45 kV, 40 mA), with Cu–K_α radiation ($\lambda = 1.5405$ Å). The samples were scanned over an angular range of $15° < 2\theta < 75°$ with 0.02° scanning step and speed of 1°/min. The XRD patterns were analyzed using X'pert HighScore software to identify the phases present in each sample. Rietveld refinement of the XRD patterns for all fabricated samples was carried out using FullProf suite 2000 software to obtain the values of refined structural parameters.

Samples for Mössbauer spectroscopy studies were prepared by gently pressing a thin layer of the powdered sample between two circular Teflon disks with diameter 2 cm, which is small compared with the distance between the γ-ray source and the sample, in order to avoid the angular broadening of the spectrum. Room temperature (RT) Mössbauer spectra were collected using a standard constant acceleration Mössbauer spectrometer over 1024 channels. The γ-ray source was a 50-mCi ^{57}Co in a rhodium matrix. The spectra were then analyzed using fitting routines based on least-squares analysis.

The magnetic measurements were carried out using a vibrating sample magnetometer (VSM MicroMag 3900, Princeton Measurements Cooperation), providing a maximum applied magnetic field of 10 kOe (1 Oe = 79.5775 A/m). The measurements were performed at room temperature.

Differential scanning calorimetry (DSC) was used to obtain quantitative and qualitative information about phase transitions involving endothermic or exothermic processes, or changes in the heat capacity of the sample under investigation. This technique was therefore employed to investigate the phase transitions and related critical temperatures of the prepared garnets using a NETZSCH–Gerätebau GmbH 204 F1 Phoenix calorimeter. The DSC measurements were performed in a temperature range from 30 °C to 350 °C at a heating rate of 5 °C per minute.

3. Results and discussion

The structural characteristics of all $Y_{3-x}Dy_xFe_5O_{12}$ samples are investigated using XRD measurements. Rietveld analysis of the diffraction patterns (shown in Fig. 1) is carried out to obtain the refined structural parameters of crystalline phases in the samples, and the refined structural results are summarized in Table 1. Figure 1 indicates that all samples reveal the presence of a single garnet phase, crystallizing in a body-centered cubic (BCC) structure with O_h^{10}-Ia3d space group. The lattice parameter a of the two end compounds ($Y_3Fe_5O_{12}$ and $Dy_3Fe_5O_{12}$) is in very good agreement with previously reported values[6] and the low values of χ^2 obtained from the Rietveld analysis indicate good agreement between the theoretical pattern (black continuous line) and the experimental data (red dots), where the line in blue representing the residual difference between the observed and calculated patterns, was a straight horizontal line with small ripples for all samples. Moreover, the enlarged views of the patterns of the two end compounds (Fig. 2) reveal that the two samples are crystallographically identical, indicating a complete substitution of Dy^{3+} ions at the Y^{3+} sites.

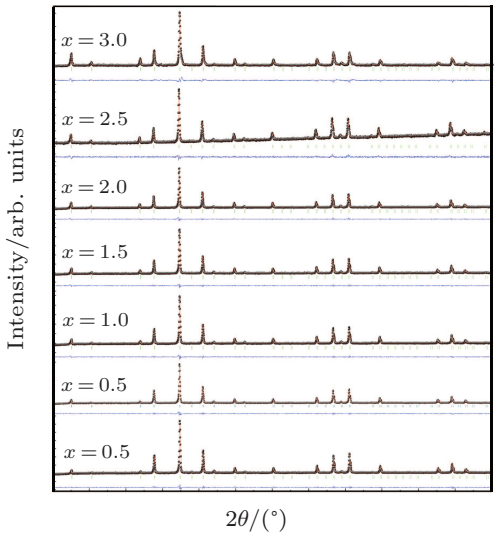


Fig. 1. (color online) Refined XRD patterns for $Y_{3-x}Dy_xFe_5O_{12}$ samples.

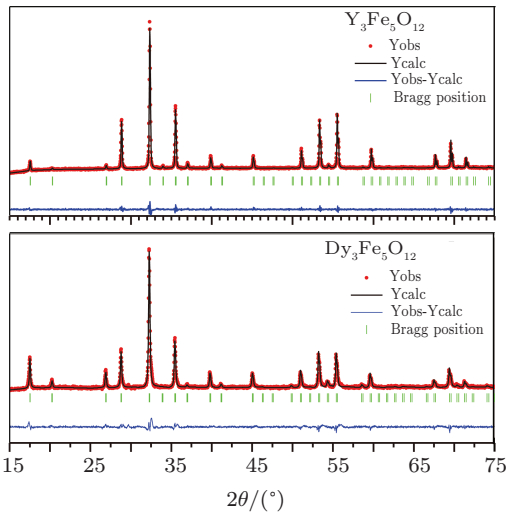


Fig. 2. (color online) Refined XRD patterns for samples $Y_{3-x}Dy_xFe_5O_{12}$ with $x = 0$ and $x = 3$, with residual difference between the experimental and calculated data given in the lower part of the plots (blue line).

Table 1. Lattice constant a, unit cell volume V, χ^2, and x-ray density ρ_x of $Y_{3-x}Dy_xFe_5O_{12}$ garnets.

Composition x	χ^2	a/Å	V/Å^3	ρ_x/(g/cm^3) (±0.01)
$Y_3Fe_5O_{12}$	1.81	12.373(4)	1894.4	5.18
$Dy_{0.5}Y_{2.5}Fe_5O_{12}$	1.90	12.376(9)	1896.0	5.43
$Dy_{1.0}Y_{2.0}Fe_5O_{12}$	1.67	12.383(8)	1899.2	5.68
$Dy_{1.5}Y_{1.5}Fe_5O_{12}$	1.56	12.390(5)	1902.3	5.92
$Dy_{2.0}Y_{1.0}Fe_5O_{12}$	1.68	12.394(7)	1904.2	6.18
$Dy_{2.5}Y_{0.5}Fe_5O_{12}$	1.15	12.409(1)	1910.8	6.41
$Dy_3Fe_5O_{12}$	2.63	12.400(9)	1907.0	6.68

The data in Table 1 reveal that the lattice parameter a and the cell volume increase with the Dy^{3+} substitution increasing, which can be attributed to the fact that the ionic radius of Dy^{3+} (1.027 Å) is greater than that of Y^{3+} (1.019 Å) at dodecahedral sites.[15] The monotonic increase of the x-ray density with increasing x, however, is opposite to what is expected based on the increase of the cell volume. This behavior can be associated with the increase of the molecular weight of the compound with Dy^{3+} substitution level increasing. The x-ray density is defined as

$$\rho_x = \frac{ZM}{N_A V}, \tag{1}$$

where $Z\,(=8)$ is the number of formula units in a unit cell, M is the molecular weight, $N_A = 6.023 \times 10^{23}$ is Avogadro's number, and V is the cell volume. Further, the molecular weight can be calculated from the atomic weights of the constituents of the molecule, which turns out to be

$$M = 738.0 + 73.6x. \tag{2}$$

Combining Eqs. (1) and (2) one can expect that a plot of $\rho_x N_A V/8$ versus x should yield a perfect straight line. Such a plot is shown in Fig. 3, where the linear fit to the experimental data presents an intercept of about 738.5 and a slope of about 73.5 (see the inset table in Fig. 3), which are in excellent agreement with the theoretical values in Eq. (2). This is an indication that the behaviors of the cell volume and x-ray density can be well explained on the basis of the statistical distribution of Dy^{3+} ions at the 24c sites.

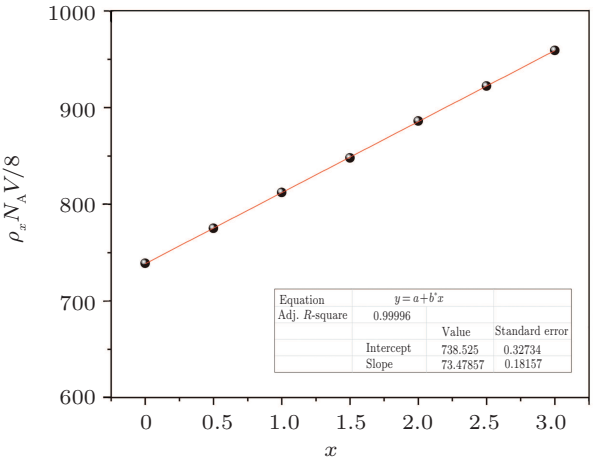


Fig. 3. (color online) Linear increase of the product of the x-ray density and cell volume with x value increasing.

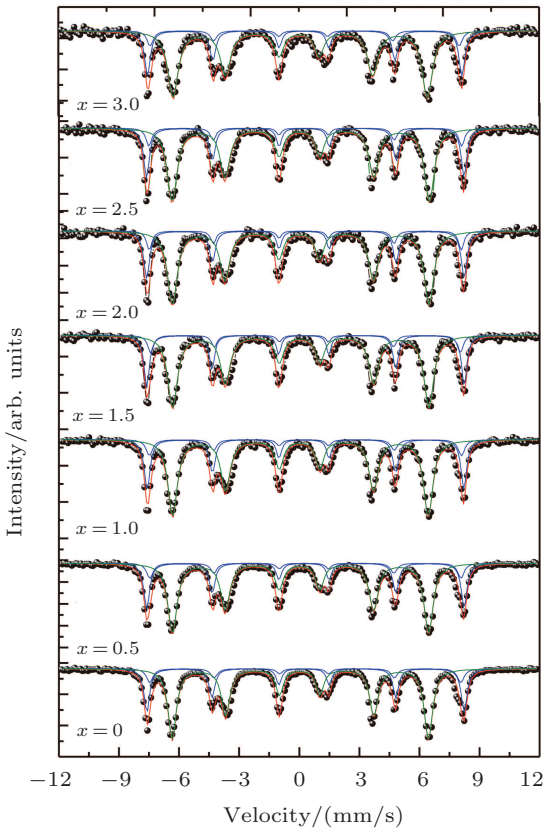


Fig. 4. (color online) Mössbauer spectra for $Y_{3-x}Dy_xFe_5O_{12}$ samples (solid circles) together with theoretical spectra obtained from fitting software (red solid curves). Components corresponding to octahedral sites are represented by blue curves, while the component corresponding to tetrahedral sites is represented by green curves.

Figure 4 shows Mössbauer absorption spectra of all $Y_{3-x}Dy_xFe_5O_{12}$ samples, and the hyperfine parameters are

listed in Table 2. These parameters are obtained by fitting Mössbauer spectra with three magnetic sextets, two of which correspond to Fe^{3+} ions at two non-equivalent octahedral ($16a$) sites, and one corresponds to Fe^{3+} ions at the tetrahedral ($24d$) site. The intensity ratio of the components associated with the octahedral sites to that with the tetrahedral site does not deviate from the value of ~37:63 for each of all compounds, which is in good agreement with the theoretical ratio of 2:3. The hyperfine fields of the Dy^{3+} substituted compounds do not deviate appreciably from the value of $B_{hf} = 497$ kOe nor 487 kOe nor $B_{hf} = 401$ kOe for the pure YIG. This is an indication that the *a*–*d* superexchange interactions between Fe^{3+} ions at the octahedral and tetrahedral site are much stronger than *ca* or *cd* interactions between Fe^{3+} and rare-earth ions.[1] The difference in hyperfine field between the two sublattices is due to the difference in the number of O^{2-} ions coordinated with Fe^{+3} ions in the octahedral sites and tetrahedral site of the iron garnet crystal lattice. In addition, the values of the center shifts (isomer shifts) are nearly the same for all samples. In view of the fact that the center shift is dependent on the s-electronic density at the nucleus,[16] the constancy of the center shifts for the octahedral sublattice (0.38 ± 0.02 mm/s) and tetrahedral sublattice (0.15 ± 0.02 mm/s) is an indication that the substitution of Y^{3+} ions by Dy^{3+} ions does not perturb the wave function of the Fe^{3+} ions, which is a further indication of the weak *c*–*a* and *c*–*d* coupling. This conclusion is also supported by the fact that the observed average hyperfine field of the octahedral sites (~492 kOe) and that of the tetrahedral site (~401 kOe) are practically equal to those of 492 kOe–495 kOe and 397 kOe–399 kOe, respectively, for Ho-substituted YIG.[14]

Table 2. Hyperfine parameters and percentage relative intensity (I) values obtained at room temperature for the $Y_{3-x}Dy_xFe_5O_{12}$ samples.

Site	B_{hf}/kOe (±5)	CS/(mm/s) (±002)	Width/(mm/s) (±003)	I/% (±2)
		$x = 0$		
Octahedral(s)	497	0.38	0.35	27
	487	0.38	0.39	10
Tetrahedral	401	0.15	0.50	63
		$x = 0.5$		
Octahedral(s)	497	0.38	0.35	27
	487	0.38	0.39	10
Tetrahedral	401	0.15	0.54	63
		$x = 1.0$		
Octahedral(s)	496	0.38	0.29	27
	488	0.38	0.30	10
Tetrahedral	400	0.16	0.55	63
		$x = 1.5$		
Octahedral(s)	497	0.38	0.32	27
	485	0.38	0.34	10
Tetrahedral	401	0.16	0.57	63
		$x = 2.0$		
Octahedral(s)	497	0.38	0.35	27
	488	0.38	0.32	10
Tetrahedral	402	0.16	0.58	63
		$x = 2.5$		
Octahedral(s)	497	0.38	0.34	27
	489	0.37	0.34	10
Tetrahedral	403	0.16	0.58	63
		$x = 3.0$		
Octahedral(s)	492	0.39	0.35	26
	484	0.37	0.38	10
Tetrahedral	398	0.16	0.62	64

The hysteresis loops (Fig. 5) indicate that all samples of $Y_{3-x}Dy_xFe_5O_{12}$ are soft magnetic materials each with a very small coercivity. Also, the loops indicate that the saturation magnetization decreases monotonically with Dy^{3+} concentration increasing. As a consequence of the *a*–*d* superexchange interaction between Fe^{3+} ions being much stronger

than the superexchange interaction between the Fe^{3+} ion and the magnetic rare-earth ion,[1,6] the net magnetization of the iron sublattices couples antiferromagnetically with the c sublattice containing the rare earth ions, and the net magnetization of the compound is given by[6]

$$M(T) = M_d(T) - M_a(T) - M_c(T). \quad (3)$$

At 0 K, the saturation magnetization of $Dy_3Fe_5O_{12}$ ($\sim$ 98 emu/g) is significantly higher than that of YIG (˜38 emu/g), indicating that the substitution of Dy^{3+} for Y^{3+} should increase the saturation magnetization at 0 K. However, due to the difference in temperature dependence between the net iron moment and the rare-earth moment, the magnetization of the compound drops sharply with temperature increasing, and becomes zero at the compensation point T_{comp} ($=$ 220 K for $Dy_3Fe_5O_{12}$). Above the compensation temperature, the magnetization increases slowly and reaches $\sim$ 5 emu/g at 300 K. Since this value is significantly lower than the saturation magnetization of $\sim$ 27 emu/g for YIG at 300 K, the following simple magnetic dilution model is proposed to explain the monotonic decrease of the RT saturation magnetization with x increasing.

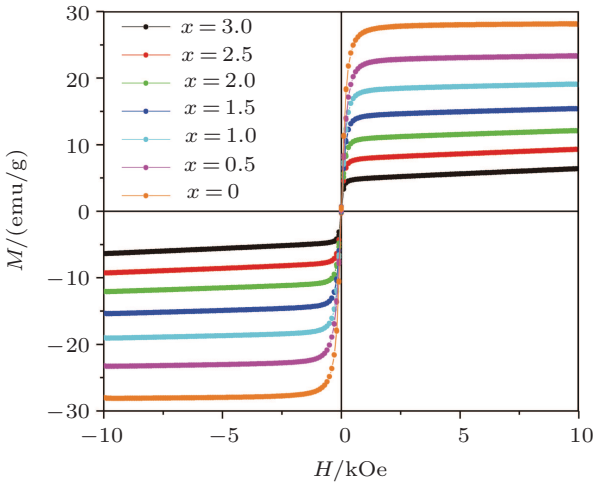


Fig. 5. (color online) Hysteresis loops for $Y_{3-x}Dy_xFe_5O_{12}$ samples.

Assuming phase separation in the Dy-substituted compound into two separated garnets according to the formula:

$$Y_{3-x}Dy_xFe_5O_{12} = \frac{3-x}{3}[Y_3Fe_5O_{12}] + \frac{x}{3}[Dy_3Fe_5O_{12}] \quad (4)$$

and using the molecular weights of 737.97 for YIG and 958.74 for $Dy_3Fe_5O_{12}$, the saturation magnetization of the general compound is calculated by using the observed RT saturation magnetizations of 28.3 emu/g[17,18] and 7.65 emu/g for the two end compounds. After some mathematical manipulation this is given by

$$(10+x)M_s = 283.8 - 61.4x. \quad (5)$$

A plot (Fig. 6) of the left-hand term of Eq. (5) versus x gives a straight line with an intercept of $\sim$ 280 and a slope of -60.7. These values are in very good agreement with the calculated values from Eq. (5), indicating that the behavior of the saturation magnetization is well described by the proposed simple magnetic dilution model, resulting from the statistical distribution of the Dy^{3+} ions in the c sublattice, which was confirmed earlier by the behavior of the x-ray density and cell volume.

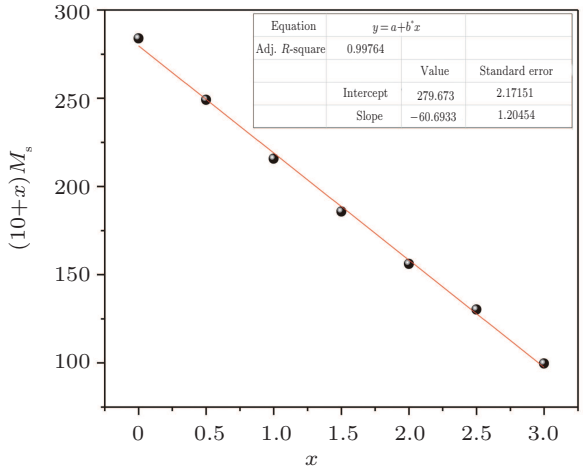


Fig. 6. (color online) Illustration of saturation magnetization behavior with Dy concentration (x) increasing.

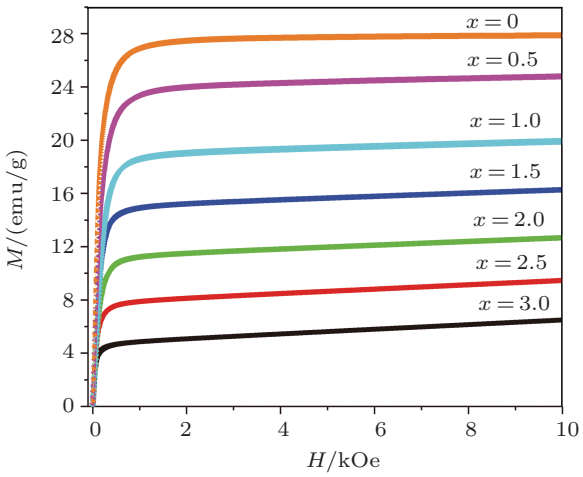


Fig. 7. (color online) Initial magnetization curves of $Y_{3-x}Dy_xFe_5O_{12}$ garnets.

The initial magnetization curves (Fig. 7) of the samples of $Y_{3-x}Dy_xFe_5O_{12}$ show that both the initial magnetic susceptibility χ_{in} and saturation magnetization M_s decrease with rare earth substitution increasing. Figure 8 shows a plot of the observed M_s [in units (emu/g)] and χ_{in} [in units (emu/g·Oe)] as a function of dysprosium concentration x. The saturation magnetization exhibits nearly a linear decrease with x increasing, which is in agreement with the reported behavior of the saturation magnetization of $Y_{3-x}Dy_xFe_5O_{12}$ ($0 \le x \le 1$) prepared by the sol–gel method.[11] On the other hand, χ_{in} shows a sharp decrease with x increasing from $x = 0$ to $x = 1$, and a slow decreasing tendency with fluctuations for x greater than 1.0.

The weakening of the magnetic parameters with Dy substitution is a consequence of the weak antiferromagnetic coupling between the RE magnetic sublattice and the net magnetization of the Fe sublattices, which leads to a sharper drop of the RE-sublattice magnetization (in comparison with the decrease of the magnetization of the Fe sublattices) as the temperature increases toward room temperature.[19]

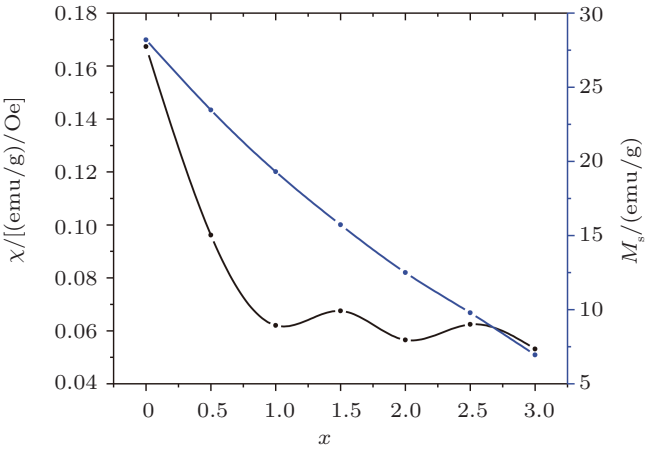


Fig. 8. (color online) Saturation magnetization M_s and initial magnetic susceptibility χ_{in} as a function of x for $Y_{3-x}Dy_xFe_5O_{12}$ garnets.

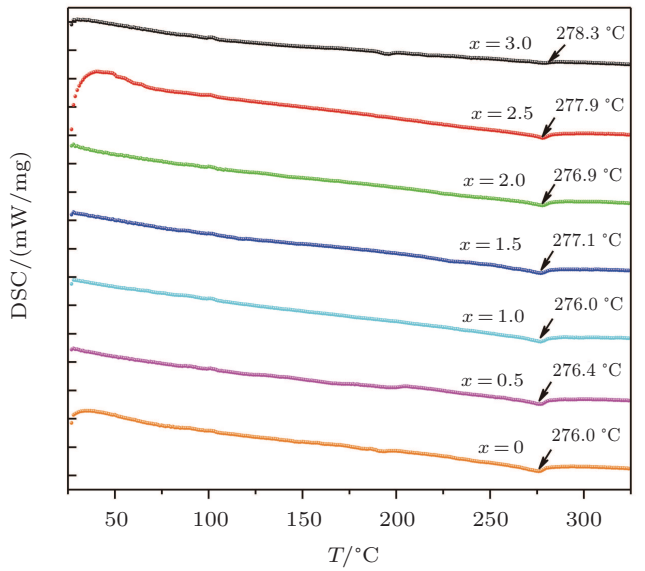


Fig. 9. (color online) DSC versus T curves of $Y_{3-x}Dy_xFe_5O_{12}$ garnets.

Differential scanning calorimetry (DSC) measurements are performed on all samples and the results are illustrated in Fig. 9. The thermal curves of all samples are almost smooth with small kinks (marked by arrows) in a temperature range of 275 °C $< T <$ 280 °C. Since abrupt changes in the thermal curves are usually associated with structural phase transitions or changes of the specific heat of the material under investigation, the positions of the small kinks in the thermal curves can be associated with temperatures at which the samples must have passed through transitions between phases with slightly different specific heats. In view of the fact that the magnetic contribution to the specific heat is rather small as reported for other magnetic oxides,[20] the observed kink in the thermal curve is associated with the Curie temperature at which ferrimagnetic–paramagnetic phase transition takes place.

The T_c values for $Y_3Fe_5O_{12}$ and $Dy_3Fe_5O_{12}$ (276.0 °C and 278.3 °C, respectively) are in good agreement with previous experimental results on rare earth iron garnets.[6] Further, T_c does not seem to change appreciably with Dy concentration, and did not differ from the values found previously for $Gd_{3-x}Er_xFe_5O_{12}$ either,[21] indicating that T_c is independent of rare-earth substitution and is determined only by the strong superexchange interaction between the two iron sublattices. If, however, we believe the small increase of T_c (from 276.0 °C to 278.3 °C) with x increasing, this increase could then be attributed to the slight strengthening of the superexchange interactions as a result of the additional weak interaction between the RE and Fe sublattices.

4. Conclusions

Dy-substituted YIG garnets are successfully synthesized by using the conventional solid state reaction method, where XRD patterns reveal the presence of a single garnet phase in each sample with no secondary phases. The lattice constant a and cell volume V increase with increasing Dy^{3+} substitution for Y^{3+} due to the larger ionic radius of Dy^{3+}, whereas the increase of the molecular mass is responsible for the observed increase of the x-ray density of the substituted compound. RT Mössbauer spectra indicate that the substitution of Dy^{3+} for Y^{3+} at the dodecahedral c site does not perturb the Fe^{3+} wave function appreciably, keeping the hyperfine parameters practically unchanged. The saturation magnetization decreases almost linearly with Dy^{3+} substitution increasing, which is explained in terms of a simple magnetic dilution model. The Curie temperature determined from the DSC measurements is found to be nearly the same for all Dy substituted compounds.

Acknowledgment

The authors Mahdi Lataifeh and Ibrahim Abu-Aljarayesh would like to thank the Deanship of Research and Graduate Studies of Yarmouk University under Garnet No. 33 /2015 used to execute part of the measurements (XRD and the thermal differential scanning calorimetry measurements) at Jordan University of Science and Technology.

References

[1] Özgür Ü, Alivov Y and Morkoç H 2009 *J. Mater. Sci. Mater. Electron.* **20** 789

[2] Özgür Ü, Alivov Y and Morkoç H 2009 *J. Mater. Sci. Mater. Electron.* **20** 911

[3] Mahmood S H and Abu-Aljarayesh I (eds.) 2016 *Hexaferrite Permanent Magnetic Materials, Materials Research Forum LLC* (Millersville: PA) p. 153

[4] Paoletti A 1978 *Physics of Magnetic Garnets: Proceedings of the International School of Physics ' Enrico Fermi', Course LXX*, Varenna on Lake Como, Villa Monastero, 27th June–9th July 1977 (Elsevier Science & Technology)

[5] Winkler G D 1981 *Magnetic garnets/Gerhard Winkler*, Vieweg, Braunschweig

[6] Gilleo M A 1980 "Ferromagnetic insulators: Garnets", in: P E Wohlfarth (ed.) *Ferromagnetic materials* (Amstrdam: North-Holland) p. 1

[7] Parida S, Rakshit S and Singh Z 2008 *J. Solid State Chem.* **181** 101

[8] Lataifeh M S 2008 *Appl. Phys. A* **92** 681

[9] Lataifeh M S and Al-sharif A 1995 *Appl. Phys. A* **61** 415

[10] Lataifeh M and McCausland M 1994 *Mu'tah Lil-Buhooth Wa Al-Dirasat* **9** 23

[11] Cheng Z, Yang H, Cui Y, Yu L, Zhao X and Feng S 2007 *J. Magn. Magn. Mater.* **308** 5

[12] Xu H and Yang H 2007 *Phys. Status Solidi A* **204** 1203

[13] Lataifeh M S and Lehlooh A F D 1996 *Solid State Commun.* **97** 805

[14] Lataifeh M S, Mahmood S and Thomas M F 2002 *Physica B: Condens. Matter* **321** 143

[15] Shannon R T 1976 *Acta Cryst. A* **32** 751

[16] Omari I, Saleh A S and Mahmood S H 1989 *J. Magn. Magn. Mater.* **78** 183

[17] Xu H, Yang H, Xu W and Yu L 2008 *Curr. Appl. Phys.* **8** 1

[18] Bouziane K, Yousif A, Widatallah H M and Amighian J 2008 *J. Magn. Magn. Mater.* **320** 2330

[19] Smit J and Wijn H P J 1959 *Ferrites* (New York: Wiley)

[20] Turki D, Remenyi G, Mahmood S, Hlil E, Ellouze M and Halouani F 2016 *Mater. Res. Bull.* **84** 245

[21] Mohaidat Q I, Lataifeh M, Mahmood S H, Bsoul I and Awawdeh M 2017 *J. Supercond. Novelmagn.* **30** 2135